Nanoscale

PAPER

View Article Online
View Journal | View Issue



Cite this: *Nanoscale*, 2024, **16**, 21326

# One-pot synthesis of heterostructured $CsPbBr_3$/PdSe nanowires with excellent humidity stability†

Shuai Ye, [a,b] Mingyi Huang,[a] Jun Song *[a,b] and Junle Qu *[a,b]

Received 30th August 2024,
Accepted 18th October 2024

DOI: 10.1039/d4nr03554b

rsc.li/nanoscale

Lead halide perovskite nanowires (NWs) have garnered increasing attention owing to their unique properties, including axial carrier transportation, low pumping thresholds, and polarized emission. However, their intrinsic instability significantly limits their applications. In this study, heterostructured $CsPbBr_3$/PbSe NWs with a diameter of 10 nm and lengths ranging from several to tens of microns were successfully synthesized *via* a one-pot solution-phase process. Photoluminescence measurements revealed that the $CsPbBr_3$/PbSe NWs emitted green fluorescence with a narrow width of 16 nm and a high photoluminescence quantum yield (PLQY) of 37.6%. The obtained $CsPbBr_3$/PbSe NWs underwent anion exchange with $I^-$ ion precursors to transform into $CsPbBr_{3-x}I_x$/PbSe, but not with $Cl^-$ ion precursors. Remarkably, these heterostructured $CsPbBr_3$/PbSe NWs remained stable when immersed in water or exposed to air for several months, demonstrating excellent humidity stability. This study offers an effective approach for preparing stable $CsPbBr_3$ NWs and fosters their future applications in optoelectronic devices.



## Introduction

Lead halide perovskite nanocrystals (NCs) represent one of the most promising materials for optoelectronic applications due to their exceptional properties.[1–5] Significant advancements have been achieved in synthesizing perovskite NCs with diverse morphologies, including 0D quantum dots (QDs),[6,7] 1D nanowires (NWs),[8] and 2D nanoplates (NPs).[9] Among these, 1D NWs have garnered considerable attention owing to their unique characteristics such as axial carrier transport, low pumping thresholds, and polarized emission, demonstrating substantial potential in applications such as photodetectors, lasers, and X-ray scintillators.[10–13] However, perovskite NCs face challenges in maintaining stability over extended periods in polar solvents, moisture, or high temperatures due to their ionic nature.[14,15] The intrinsic instability of lead-halide perovskites severely limits their practical applications, necessitating urgent solutions.

Numerous studies have been conducted in the past decade to enhance the stability of perovskite NCs. For instance, all-inorganic perovskite QDs ($CsPbX_3$) have been extensively explored. Common strategies for enhancing the stability of $CsPbX_3$ QDs involve their encapsulation within a hydrophobic matrix or coating with protective shells, isolating them from the surrounding environment.[16,17] More recently, a variety of heterostructured $CsPbX_3$ QDs have been developed, significantly improving their stability.[18–20] These heterostructured $CsPbX_3$ QDs are typically synthesized using straightforward methods. For instance, Zhang *et al.* employed an effective sol–gel process to prepare $CsPbX_3$-based heterostructures with $ZrO_2$ or $SiO_2$.[21,22] Wang *et al.* sulfureted the surface of $CsPbX_3$ QDs with hexamethyldisilathiane at room temperature to produce heterostructured $CsPbX_3$–PbS (X = Cl, Br, I) QDs.[23] Manna *et al.* reported a simple hot-injection method for fabricating $CsPbX_3$–$Pb_4S_3Br_2$ QDs heterostructures.[24]

These successful strategies for fabricating $CsPbX_3$ QDs can also enhance the stability of $CsPbX_3$ NWs. However, relatively few related studies have been conducted to date. Core–shell $CsPbBr_3$/$MoO_3$ NWs were synthesized by a vapor–liquid–solid (VLS) process.[25] The $MoO_3$ shell effectively passivated the surface of the $CsPbBr_3$ NW cores, thereby reducing the diffusion of harmful water and oxygen molecules and enhancing air stability. Additionally, core–shell PbSe@$CsPbBr_3$ wire heterostructures were prepared through conformal epitaxy of a $CsPbBr_3$ shell on a PbSe wire core using chemical vapor deposition (CVD).[26] Compared to the VLS and CVD processes, the solution-phase process is simpler, more economical, and

[a]*State Key Laboratory of Radio Frequency Heterogeneous Integration (Shenzhen University); College of Physics and Optoelectronic Engineering, Key Laboratory of Optoelectronic Devices and Systems of Ministry of Education and Guangdong Province, Shenzhen University, Shenzhen 518060, P. R. China. E-mail: songjun@szu.edu.cn*

[b]*Medical Engineering and Technology College, Xinjiang Medical University, Urumqi 830011, P. R. China. E-mail: jlqu@szu.edu.cn*

† Electronic supplementary information (ESI) available. See DOI: https://doi.org/10.1039/d4nr03554b

widely used for preparing perovskite NWs. Here, we propose a one-pot strategy for synthesizing heterostructured $CsPbBr_3$/PbSe NWs using a solution-phase process. The resulting $CsPbBr_3$/PbSe NWs had a diameter of approximately 10 nm and lengths ranging from several to tens of microns. They remained stable even after immersion in water or exposure to air for several months, exhibiting excellent humidity stability.

## Experimental

### Materials

$PbCl_2$ (99.999%), $PbBr_2$ (99.999% pure), $PbI_2$ (99.999% pure), $Cs_2CO_3$ (99.9%), 1-octadecene (ODE, 90%), oleic acid (OA, 90%), oleylamine (OLA, 70% pure), 1-dodecanethiol (DDT, 99.9%) and selenium powders (Se, 99.999%) were purchased from Sigma-Aldrich (St Louis, MO, USA). Analytical hexane was purchased from Macklin Biochemical Co., Ltd (Shanghai, China). All chemicals were used without further purification.

### Preparation of Pb precursor solution

0.3 mmol of $PbBr_2$ powders was added to a 50 ml stand-up flask containing 5 mL of ODE, 0.25 mL of OA, and 0.5 mL of OLA. The flask was heated to 160 °C in a flowing argon atmosphere under vigorous stirring until the $PbBr_2$ powders were dissolved completely. Then, the obtained Pb/Br precursor solution was cooled to room temperature and stored for subsequent use. The Pb/Cl precursor solution and Pb/I precursor solution were prepared by a similar process.

### Preparation of Cs precursor solution

0.1 mmol of $Cs_2CO_3$ powders was added to a 50 ml stand-up flask containing 5 mL of ODE and 0.25 mL of OA. The flask was heated to 160 °C in a flowing argon atmosphere under vigorous stirring until the $Cs_2CO_3$ powders were dissolved completely. Then, the obtained solution was cooled to room temperature and stored for subsequent use.

### Preparation of Se solution

The Se solution was prepared by a previous approach developed by Yang *et al.* 1.5 mmol of Se powders were added to a brown vial containing 0.75 ml of DDT and 0.75 ml of OLA. The mixture in the vial was stirred vigorously using a magnetic bar at room temperature for more than 4 hours. The Se powders were dissolved completely and the Se solution was obtained.

### Preparation of $CsPbBr_3$/PbSe nanowires (NWs)

5.75 ml of Pb/Br precursor solution, 5.25 ml of Cs precursor solution and 30 μl of Se solution were simultaneously added to a 50 ml stand-up flask at room temperature. Note that an additional 0.5 ml of OA and 0.5 ml of OLA must be added to prepare the $CsPbBr_3$/PbSe NWs. The mixed solutions were stirred under a flowing Ar atmosphere and then heated quickly to 160 °C (~5 min). After maintaining the temperature for 20 min at 160 °C, the reacted flask was allowed to cool naturally to room temperature. The crude solutions were centrifuged at 10 000 rpm for 10 min to precipitate the products. The supernatants were removed and the precipitates were dispersed in 10 mL of hexane. The dispersed solution was centrifuged at 1000 rpm for 10 min to precipitate the $CsPbBr_3$/PbSe NWs. Finally, the collected $CsPbBr_3$/PbSe NWs were dispersed in 10 mL of hexane again and stored for subsequent use.

### Characterization

An X-ray diffractometer (XRD, X'Pert PRO, Netherlands) with Cu Kα radiation was used to analyze the microstructures of the NWs. Transmission electron microscopy (TEM, JEM-T7700, Japan) was used to observe the samples' morphologies. Ultraviolet/visible (UV/vis) absorption spectra were recorded using a spectrophotometer (U-2800, Hitachi, Japan). Photoluminescence (PL) spectra were recorded and time-resolved fluorescence measurements were taken with a Fluorolog®-3 spectrofluorometer (HORIBA Scientific, Japan). The photoluminescent quantum yield (PLQY) was also measured with the Fluorolog®-3 spectrofluorometer by direct methods. All spectra were measured at room temperature in a quartz cuvette.

## Results and discussion

To synthesize the $CsPbBr_3$/PbSe NWs, $PbBr_2$ and $Cs_2CO_3$ powders were pre-dissolved in ODE/OA/OLA and ODE/OA, respectively, to prepare the precursor solutions. The Pb precursor, Cs precursor, and OLA/DDT solutions with dissolved Se were then mixed simultaneously at room temperature; subsequently, the mixture was rapidly heated to 160 °C and the reaction was maintained for 20 min. Notably, the amounts of OA and OLA needed to be adjusted to control the morphologies of the products. The detailed procedure is described in the ESI.† Three crucial factors must be considered when preparing the $CsPbBr_3$/PbSe NWs. The first is the reaction precursor: $CsPbBr_3$/PbSe NWs are only produced when the pre-dissolved Pb precursor, Cs precursor, and OLA/DDT solutions with dissolved Se are simultaneously mixed at room temperature. $CsPbBr_3$ nanocubes and nanorods are produced when the precursors are $PbBr_2$ and $Cs_2CO_3$ powders, respectively (Fig. S1†). A similar process was used in the solvothermal process for preparation of $CsPbX_3$ NCs.[27] The second factor is the stoichiometric ratio of OA to OLA: products with a high content of $CsPbBr_3$/PbSe NWs are obtained when 1 ml of OA and 1 ml of OLA are used (Fig. S2, S3 and Table S1†). The last factor is the addition of DDT and Se: synthesizing $CsPbBr_3$/PbSe NWs in the absence of DDT or Se in the initial solution is challenging (Fig. S4†).

The formation mechanism of $CsPbBr_3$/PbSe NWs was investigated initially. Samples were quenched at various stages during the preparation process, and their morphologies and absorption spectra were analyzed (see Fig. 1 and S5, and Table S2†). During the heating stage from room temperature to 160 °C (Fig. 1a–e), the products exhibited diverse mor-

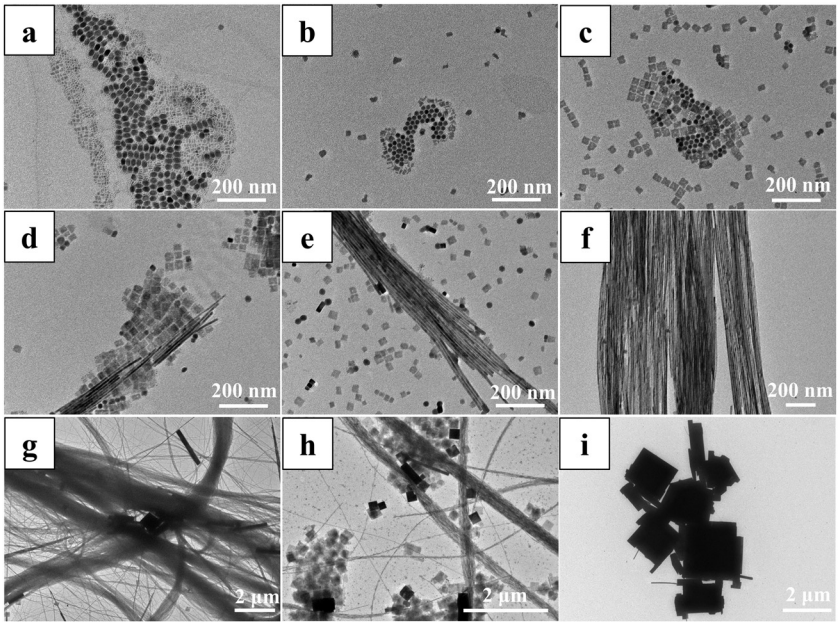


**Fig. 1** TEM images of samples quenched at different times during the transformation from the precursor solution into NWs: (a) 80 °C, (b) 100 °C, (c) 120 °C, (d) 140 °C, (e) 160 °C, 0 min, (f) 160 °C, 20 min, (g) 160 °C, 30 min, (h) 160 °C, 60 min, and (i) 160 °C, 90 min.

phologies at different temperatures. Products quenched at 80 °C (Fig. 1a) displayed complex morphologies and non-uniform sizes, with many nanocrystals smaller than 5 nm, resulting in weak cyan fluorescence (Fig. S5a†). When the reaction temperature was increased to 100 °C (Fig. 1b), the products predominantly consisted of hexagonal nanocrystals with uniform sizes and irregularly shaped nanosheets. Analysis of the absorption spectrum (Fig. S5b†) showed a characteristic peak centered at 311 nm, suggesting that the hexagonal nanocrystals were $Cs_4PbBr_6$. Further raising the temperature to 120 °C (Fig. 1c) led to the nanosheets becoming regular squares with widths of approximately 40 nm, resulting in a change in the emission color of the products to green. Additionally, hexagonal $Cs_4PbBr_6$ nanocrystals were present. NWs several hundred nanometers in length were initially observed in products quenched at 140 °C (Fig. 1d), with their lengths increasing as the temperature was raised to 160 °C (Fig. 1e). During the heat-holding stage at 160 °C (Fig. 1f), more NWs nucleated and grew, while the hexagonal nanocrystals and square nanosheets disappeared over time. However, the NWs gradually transformed into larger crystals as the time increased beyond 20 min (Fig. 1g–i). Consequently, intermediates with various morphologies were obtained and gradually transformed under the given conditions during the formation of $CsPbBr_3$/PbSe NWs. The formation mechanism of $CsPbBr_3$/PbSe NWs closely resembled that of pure $CsPbBr_3$ NWs reported by Yang *et al.*, wherein the NWs were nucleated and grown through a surfactant-directed 1D mode, rather than by the oriented attachment of NCs or seed-mediated anisotropic growth.[28] Notably, $CsPbBr_3$/PbSe NWs were formed within 20 min, considerably faster than the time required for pure $CsPbBr_3$ NWs (90 min).

The microstructure of the colloidal $CsPbBr_3$/PbSe NWs was characterized using X-ray diffraction (XRD). The XRD pattern in Fig. 2a indicates that the synthesized NW samples exclusively comprised the $CsPbBr_3$ and PbSe phases. As is known, $CsPbBr_3$ exhibits three different phases, namely cubic, tetragonal, and orthorhombic, with phase transitions occurring at 130 °C from cubic to tetragonal and at 88 °C from tetragonal to orthorhombic.[29] The distinct double peaks at approximately 30° corresponding to the (002) and (200) lattice planes (JCPDS

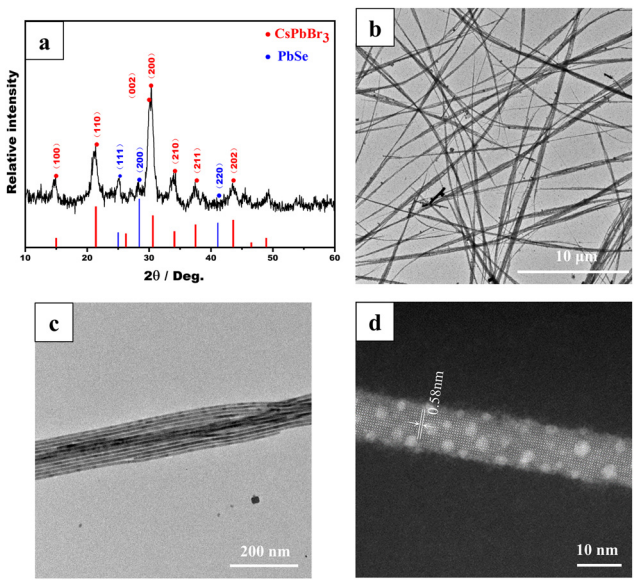


**Fig. 2** Structural characterization of colloidal $CsPbBr_3$/PbSe NWs: (a) XRD pattern, (b–c) TEM images, and (d) HAADF-STEM image.

18-0364) confirmed the orthorhombic $CsPbBr_3$ phase in the $CsPbBr_3$/PbSe NWs. Additionally, diffraction peaks at 25.1° and 28.5° corresponded to the (111) and (200) lattice planes, respectively, of the cubic PbSe phase (JCPDS 06-0354), indicating the presence of the PbSe phase. The morphologies of the $CsPbBr_3$/PbSe NWs were examined using transmission electron microscopy (TEM) (Fig. 2b and c). The synthesized $CsPbBr_3$/PbSe NWs formed bundles, with each bundle consisting of separate NWs with a uniform size of approximately 10 nm. The $CsPbBr_3$/PbSe NWs ranged from several microns to tens of microns in length. The high-resolution high-angle annular dark-field scanning TEM (HAADF-STEM) image in Fig. 2d depicted single crystal $CsPbBr_3$/PbSe NWs in the [100] direction, with an interplanar distance of ~0.58 nm corresponding to the (100) plane of $CsPbBr_3$. Furthermore, tiny PbSe nanoparticles (1–3 nm in size) were embedded in the $CsPbBr_3$ matrix. The XPS spectrum (Fig. S6†) also confirmed the coexistence of $Cs^+$, $Pb^{2+}$, $Br^-$, and the peak at 59.2 eV in the XPS spectrum was assigned to the Se 3d signals of $Se^{2-}$, indicating that $Se^{2-}$ had been incorporated into the NWs. EDS analysis (Fig. S7†) further confirmed the coexistence of Cs, Pb, Br, and Se in the $CsPbBr_3$/PbSe NWs. Another experiment involved reacting the $PbBr_2$ precursor solution solely with the Se precursor solution at 160 °C for 5 min, resulting in cubic PbSe nanoparticles with sizes in the range of 5–10 nm (Fig. S8†). This experiment confirmed the formation of PbSe nanoparticles under the reaction conditions used to prepare the $CsPbBr_3$/PbSe NWs. Combined with the aforementioned formation mechanism, it can be inferred that the nucleation and growth of $CsPbBr_3$/PbSe NWs occurred. In the early stages, $CsPbBr_3$ and PbSe seeds formed simultaneously. The number of $CsPbBr_3$ seeds was considerably higher than that of PbSe seeds due to the higher Br concentration compared to the Se concentration in the precursor solution. During the growth process of the NWs, the PbSe seeds grew into PbSe NCs and were gradually surrounded by growing $CsPbBr_3$ seeds, forming $CsPbBr_3$/PbSe heterostructures. These heterostructures inhibited the growth of PbSe NCs, resulting in a smaller size of the PbSe NCs in the $CsPbBr_3$/PbSe NWs than in the PbSe NCs (Fig. S8†).

The optical properties of the synthesized $CsPbBr_3$/PbSe NWs were characterized (Fig. 3). The absorption spectrum of $CsPbBr_3$/PbSe NWs (Fig. 3a) revealed an absorption peak at 510 nm. In contrast to the sharp edges of pure $CsPbBr_3$ QDs or NWs, an absorption tail in the long-wavelength direction was observed for $CsPbBr_3$/PbSe NWs, attributed to the growth of PbSe nanoparticles within the $CsPbBr_3$/PbSe NWs. The photoluminescence (PL) spectrum of $CsPbBr_3$/PbSe NWs displayed a single narrow emission peak at 516 nm with a width of 16 nm, similar to that of $CsPbBr_3$ QDs. The PL quantum yield of the $CsPbBr_3$/PbSe NWs was measured at 37.6% (Fig. 3b), which closely approximates the value reported for pure 10.0 nm thick $CsPbBr_3$ NWs (~38%) by Manna *et al.*[30] Time-resolved PL measurements of the $CsPbBr_3$/PbSe NWs (Fig. 3c) revealed bi-exponential decay traces, with an average lifetime of only 6.88 ns, 42% lower than that of pure 10.0 nm thick $CsPbBr_3$ NWs (16.4 ns).[30] To further investigate the optical properties, the $CsPbBr_3$/PbSe NWs were deposited onto a glass slide and imaged using confocal microscopy under excitation by a 488 nm continuous-wave laser (Fig. 3d–f). The 10 nm thick $CsPbBr_3$/PbSe NWs were sufficiently long to be observed in bright field, with strong fluorescent signals detected in the fluorescence field. The merged images in Fig. 3d and e indicate fluorescence emitted by the $CsPbBr_3$/PbSe NWs.

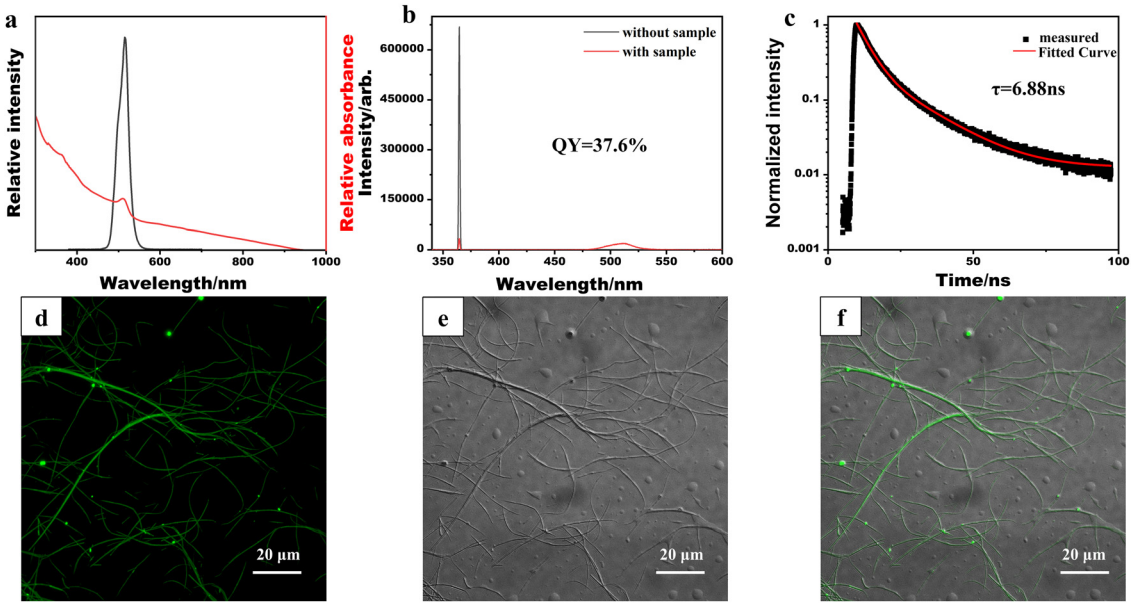


**Fig. 3** Optical characterization of $CsPbBr_3$/PbSe nanowires: (a) UV/vis absorption and photoluminescence spectra, (b) PLQY, (c) lifetime, (d) confocal fluorescence image, (e) bright field image and (f) merged image of (d) and (e).

In prior studies,[31] anion exchange was utilized to adjust the emission band of halide perovskite nanocrystals. Similarly, the emission band of the synthesized $CsPbBr_3$/PbSe NWs could be tuned *via* anion exchange. Fig. 4 illustrates the emission color changing from green to yellow to dark red as $I^-$ precursors were gradually introduced into the dispersion of $CsPbBr_3$/PbSe NWs in hexane, providing a series of tunable PL signals from 516 to 660 nm with a narrow band (FWHM in the range of 15–40 nm). Anion exchange of $CsPbBr_3$/PbSe NWs with $I^-$ ions occurred rapidly at room temperature, whereas exchange with $Cl^-$ ions was hindered. The emission color remained unchanged when $Cl^-$ precursors were added to the dispersion of $CsPbBr_3$/PbSe NWs at room temperature (Fig. S9†). Similarly, the emission color of the $CsPbBr_3$ QD dispersion quickly shifted from green to blue. This unusual phenomenon may be linked to internal strain within the $CsPbBr_3$/PbSe NWs. Incorporation of PbSe nanoparticles into the $CsPbBr_3$ matrix resulted in a 4.8% lattice mismatch, producing internal strain. Gradual release of this strain occurred upon anion exchange with $I^-$ ions due to a decreased mismatch (2.9%) with $CsPbI_3$, making the reaction easily achievable. Conversely, the 8.8% lattice mismatch between PbSe and the $CsPbCl_3$ lattice generated strong internal strain, hindering the anion exchange of $CsPbBr_3$/PbSe NWs with $Cl^-$ ions.

The integration of PbSe nanoparticles into the $CsPbBr_3$ NWs significantly enhanced their humidity stability. Fig. 5 illustrates the stability of two $CsPbBr_3$/PbSe NW samples. The sample labeled "in air" consisted of a $CsPbBr_3$/PbSe NW film coated on a glass slide and exposed to air, whereas the other sample labeled "in water" comprised centrifuged $CsPbBr_3$/PbSe NW powders immersed in a tube filled with deionized water. The $CsPbBr_3$/PbSe NWs demonstrated robust stability in both air and water (Fig. 5a). The PL intensity of the $CsPbBr_3$/PbSe NW film exposed to air retained approximately 95% of its original intensity after 30 days, while the fluorescence intensity of the $CsPbBr_3$/PbSe NW film powders immersed in deionized

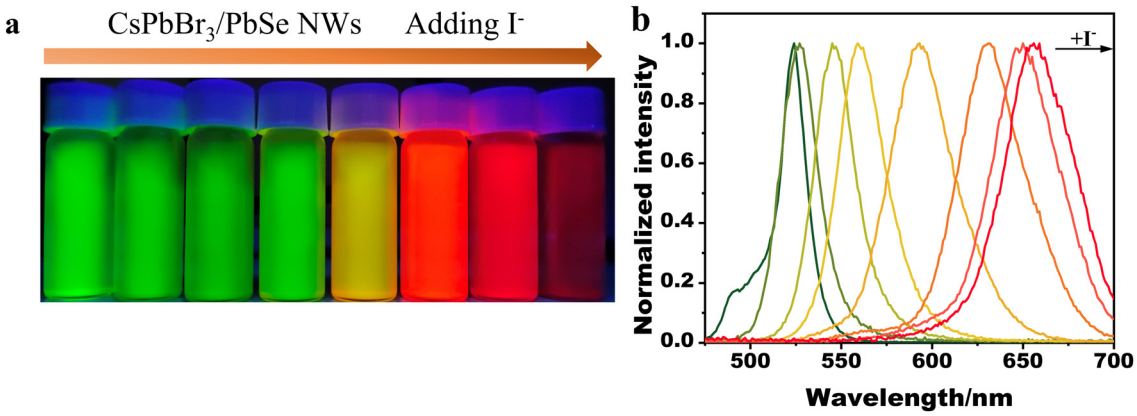


Fig. 4 (a) Photograph of colloidal $CsPbBr_3$/PbSe NWs reacting with different concentrations of $I^-$ ions under a 365 nm UV lamp; (b) corresponding photoluminescence spectra of colloidal $CsPbX_3$/PbSe perovskite NWs.

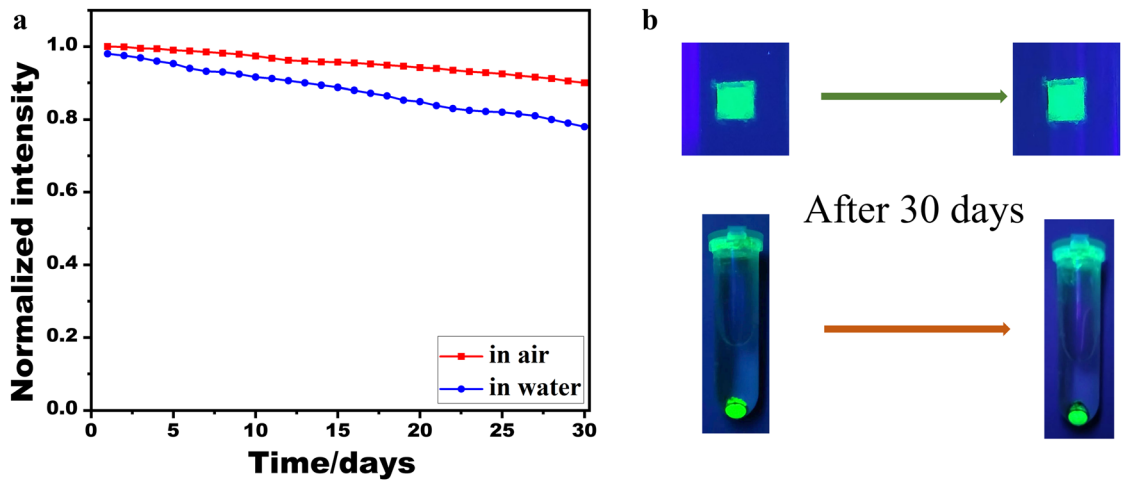


Fig. 5 (a) PL intensity change of colloidal $CsPbBr_3$/PbSe NWs in air and in water, (b) photographs of $CsPbBr_3$/PbSe NW samples under a 365 nm lamp: top is the $CsPbBr_3$/PbSe NWs film on a glass slide exposed to air, and bottom is the centrifuged $CsPbBr_3$/PbSe NWs in a tube full of deionized wate.

water retained approximately 80% of its original PL intensity after the same duration. Fig. 5b presents photographs of the two $CsPbBr_3$/PbSe NW samples under excitation by 365 nm lamps. The $CsPbBr_3$/PbSe NW sample retained its original shape when exposed to air or immersed in water for 30 days, exhibiting strong green fluorescence under the 365 nm lamp. Notably, the PL of perovskite nanocrystals is typically completely quenched within several hours of immersion in water. The results depicted in Fig. 5 indicate the excellent humidity stability of the $CsPbBr_3$/PbSe NWs. In previous research, core–shell $CsPbBr_3/MoO_3$ NWs have been developed to enhance the stability of $CsPbBr_3$ NWs.[25] The mobility of the $CsPbBr_3/MnO_3$ NWs was maintained at 80% after 7 days' storage at 65% relative humidity. Another strategy to enhance the stability of $CsPbBr_3$ NWs was to passivate their surfaces with thiourea. The passivated $CsPbBr_3$ NWs retained approximately 80% of their original performance after 2 hours of water treatment.[32] Comparatively, the $CsPbBr_3$/PbSe NWs in this work demonstrated superior stability. However, a direct comparison of the stability between $CsPbBr_3$/PbSe NWs and pure $CsPbBr_3$ NWs is not feasible due to the current process's inability to produce pure $CsPbBr_3$ NWs. To shed light on this, we refer to $CsPbX_3$ QDs. Previous studies have highlighted that the stability of $CsPbX_3$ QDs can be enhanced by incorporating metal chalcogenides such as ZnS,[33] PbS,[34] and PbTe.[35] Density functional theory (DFT) calculations[36] have revealed that the augmented stability of $CsPbX_3$ QDs primarily stems from the strong interaction and high binding energy at the interface between the perovskite and the metal chalcogenide. Additionally, in the $CsPbBr_3$ NWs passivated by thiourea,[32] the enhanced stability was attributed to the surface passivation effect of thiourea, which forms a relatively stable $Pb^{2+}$–thiourea complex with $Pb^{2+}$. In the $CsPbBr_3$/PbSe NWs, the incorporation of PbSe nanoparticles into the $CsPbBr_3$ matrix led to the formation of a stable complex and high binding energy at the interface, thus improving the stability of the $CsPbBr_3$ NWs.

## Conclusions

This study proposed a one-pot solution-phase process to synthesize heterostructured $CsPbBr_3$/PbSe NWs and successfully obtained $CsPbBr_3$/PbSe NWs with a diameter of 10 nm and lengths ranging from several to tens of microns. The $CsPbBr_3$/PbSe NWs emitted green fluorescence with a narrow width of 16 nm and a high photoluminescence quantum yield (PLQY) of 37.6%. In contrast to pure $CsPbBr_3$ NWs, the heterostructured $CsPbBr_3$/PbSe NWs only underwent anion exchange with the $I^-$ ion precursor, transforming into $CsPbBr_{3-x}I_x$/PbSe, and did not react with the $Cl^-$ ion precursor. These heterostructured $CsPbBr_3$/PbSe NWs demonstrated excellent humidity stability owing to the strong binding energy resulting from the incorporation of PbSe nanoparticles into the $CsPbBr_3$ matrix; they maintained their strong emission even when immersed in water or exposed to air for several months.

## Author contributions

J. S. conceived the overall project and supervised the effort. S. Y. and M. H. designed the experiments, ran the synthetic protocols, and characterized the samples. J. S. and J. Q. helped in data curation. S. Y. wrote the original draft with help from all the authors. J. S. and J. Q. reviewed and revised the manuscript.

## Data availability

The data supporting this article have been included as part of the ESI.†

## Conflicts of interest

The authors declare no conflict of interest.

## Acknowledgements

This study received partial support from the National Key R&D Program of China (2021YFF0502900), the National Natural Science Foundation of China (62175161/62127819), the Shenzhen Basic Research Program (JCYJ20210324095810028), and the Shenzhen Key Laboratory of Photonics and Biophotonics (ZDSYS20210623092006020). We thank the Instrument Analysis Center of Shenzhen University for their assistance with the TEM analysis.

## References

1 Q. Zhang, Q. Shang, R. Su, T. T. H. Do and Q. Xiong, *Nano Lett.*, 2021, **21**, 1903–1914.
2 D. Yang, B. Zhao, T. Yang, R. Lai, D. Lan, R. H. Friend and D. Di, *Adv. Funct. Mater.*, 2022, **32**, 2109495.
3 H.-Y. Hou, S. Tian, H.-R. Ge, J.-D. Chen, Y.-Q. Li and J.-X. Tang, *Adv. Funct. Mater.*, 2022, **32**, 2209324.
4 S. Ye, W. Yan, M. Zhao, X. Peng, J. Song and J. Qu, *Adv. Mater.*, 2018, **30**, 180016.
5 F. Zhao, A. Ren, P. Li, Y. Li, J. Wu and Z. M. Wang, *ACS Nano*, 2022, **16**, 7116–7143.
6 L. Protesescu, S. Yakunin, M. I. Bodnarchuk, F. Krieg, R. Caputo, C. H. Hendon, R. X. Yang, A. Walsh and M. V. Kovalenko, *Nano Lett.*, 2015, **15**, 3692–3696.
7 X. Li, Y. Wu, S. Zhang, B. Cai, Y. Gu, J. Song and H. Zeng, *Adv. Funct. Mater.*, 2016, **26**, 2435–2445.
8 D. Zhang, Q. Zhang, Y. Zhu, S. Poddar, Y. Zhang, L. Gu, H. Zeng and Z. Fan, *Adv. Energy Mater.*, 2023, **13**, 2201735.
9 J. Shamsi, Z. Dang, P. Bianchini, C. Canale, F. D. Stasio and R. Brescia, *J. Am. Chem. Soc.*, 2016, **138**, 7240–7243.
10 Y. Fu, H. Zhu, C. C. Stoumpos, Q. Ding, J. Wang, M. G. Kanatzidis, X. Zhu and S. Jin, *ACS Nano*, 2016, **10**, 7963–7972.

11 G. S. Kumar, R. R. Sumukam, R. K. Rajaboina, R. N. Savu, M. Srinivas and M. Banavoth, *ACS Appl. Energy Mater.*, 2022, **5**, 1342–1377.
12 Y. Meng, C. Lan, F. Li, S. Yip, R. Wei, X. Kang, X. Bu, R. Dong, H. Zhang and J. C. Ho, *ACS Nano*, 2019, **13**, 6060–6070.
13 H. Dierks, Z. Zhang, N. Lamers and J. Wallentin, *Nano Res.*, 2023, **16**(1), 1084–1089.
14 Y. Zhou and Y. Zhao, *Energy Environ. Sci.*, 2019, **12**, 1495–1511.
15 Y. Wei, Z. Cheng and J. Lin, *Chem. Soc. Rev.*, 2019, **48**, 310–350.
16 D. N. Dirin, L. Protesescu, D. Trummer, I. V. Kochetygov, S. Yakunin, F. Krumeich, N. P. Stadie and M. V. Kovalenko, *Nano Lett.*, 2016, **16**, 5866–5874.
17 Y. Wei, X. Deng, Z. Xie, X. Cai, S. Liang, P. Ma, Z. Hou, Z. Cheng and J. Lin, *Adv. Funct. Mater.*, 2017, 1703535.
18 Y. Wei, Y. Zhao, C. Liu, Z. Wang, F. Jiang, Y. Liu, Q. Zhao, D. Yu and M. Hong, *Adv. Funct. Mater.*, 2021, **31**, 2106386.
19 P. V. Kamat, N. Pradhan, K. Schanze, P. S. Weiss, J. Buriak, P. Stang, T. W. Odom and G. Hartland, *ACS Energy Lett.*, 2020, **5**, 2253–2255.
20 X. Tang, J. Yang, S. Li, Z. Liu, Z. Hu, J. Hao, J. Du, Y. Leng, H. Qin, X. Lin, Y. Lin, Y. Tian, M. Zhou and Q. Xiong, *Adv. Sci.*, 2019, **6**, 1900412.
21 H. Hu, L. Wu, Y. Tan, Q. Zhong, M. Chen, Y. Qiu, D. Yang, B. Sun, Q. Zhang and Y. Yin, *J. Am. Chem. Soc.*, 2018, **140**, 406–412.
22 H. Liu, Y. Tan, M. Cao, H. Hu, L. Wu, X. Yu, L. Wang, B. Sun and Q. Zhang, *ACS Nano*, 2019, **13**, 5366–5374.
23 X. Zhang, X. Wu, X. Liu, G. Chen, Y. Wang, J. Bao, X. Xu, X. Liu, Q. Zhang, K. Yu, W. Wei, J. Liu, J. Xu, H. Jiang, P. Wang and X. Wang, *J. Am. Chem. Soc.*, 2020, **142**, 4464–4471.
24 M. Imran, L. Peng, A. Pianetti, V. Pinchetti, J. Ramade, J. Zito, F. D. Stasio, J. Buha, S. Toso, J. Song, I. Infante, S. Bals, S. Brovelli and L. Manna, *J. Am. Chem. Soc.*, 2021, **143**, 1435–1446.
25 Y. Meng, Z. Lai, F. Li, W. Wang, S. Yip, Q. Quan, X. Bu, F. Wang, Y. Bao, T. Hosomi, T. Takahashi, K. Nagashima, T. Yanagida, J. Lu and J. C. Ho, *ACS Nano*, 2020, **14**, 12749–12760.
26 C. Fan, X. Xu, K. Yang, F. Jiang, S. Wang and Q. Zhang, *Adv. Mater.*, 2018, **30**, 1804707.
27 M. Chen, Y. Zou, L. Wu, Q. Pan, D. Yang, H. Hu, Y. Tan, Q. Zhong, Y. Xu, H. Liu, B. Sun and Q. Zhang, *Adv. Funct. Mater.*, 2017, 1701121.
28 D. Zhang, S. W. Eaton, Y. Yu, L. Dou and P. Yang, *J. Am. Chem. Soc.*, 2015, **137**, 9230–9233.
29 C. K. Moeller, *Nature*, 1958, **182**, 1436.
30 M. Imran, F. D. Stasio, Z. Dang, C. Canale, A. H. Khan, J. Shamsi, R. Brescia, M. Prato and L. Manna, *Chem. Mater.*, 2016, **28**, 6450–6454.
31 S. Ye, M. Zhao, J. Song and J. Qu, *Nano Res.*, 2018, **11**(9), 4654–4663.
32 P. Li, D. Yang, Y. Tan, M. Cao, Q. Zhong, M. Chen, H. Hu, B. Sun, Q. Zhong, M. Chen, H. Hu and B. Sun, *ACS Appl. Mater. Interfaces*, 2019, **11**, 3351–3359.
33 V. K. Ravi, S. Saikia, S. Yadav, V. V. Nawale and A. Nag, *ACS Energy Lett.*, 2020, **5**, 1794–1796.
34 M. Jagadeeswararao, P. Vashishtha, T. J. N. Hooper, A. Kanwat, J. W. M. Lim, S. K. Vishwanath, N. Yantara, T. Park, T. C. Sum, D. S. Chung, S. G. Mhaisalkar and N. Mathews, *J. Phys. Chem. Lett.*, 2021, **12**, 9569–9578.
35 L. Zhang, M. Zhu, Y. Sun, J. Zhang, M. Zhang, H. Zhang, F. Zhou, J. Qu and J. Song, *Nano Energy*, 2021, **90**, 106506.
36 W. Chen, J. Hao, W. Hu, Z. Zang, X. Tang, L. Fang, T. Niu and M. Zhou, *Small*, 2017, **13**, 1604085.